PHYSICAL REVIEW VOLUME 184, NUMBER 3 15 AUGUST 1969

Shallow Donor Electrons in Silicon. I. Hyperfine Interactions from ENDOR Measurements*

EDWARD B. HALE† AND ROBERT LEE MIEHER‡
Department of Physics, Purdue University, Lafayette, Indiana 47907

(Received 17 March 1969)

The hyperfine interactions of Si^{29} lattice nuclei with ground-state donor electrons in arsenic-, phosphorus-, and antimony-doped silicon have been measured by electron-nuclear double resonance (ENDOR). Hyperfine constants are reported for each donor for about 20 shells containing a total of about 150 lattice nuclei. About 15 of these shells per donor are reported for the first time; five were reported previously. Our results differ significantly for shells D and E; the other three shells were measured with greater accuracy. The matching of experimental hyperfine tensors to their lattice sites cannot be readily determined. A systematic technique used to analyze the ENDOR spectra is discussed.

I. INTRODUCTION

A DONOR electron occurs when a Group-V impurity atom substitutes at a normal silicon lattice site. Of the five valence electrons belonging to the impurity, four become tightly bound in the normal lattice tetrahedral bonds; the fifth, or donor electron, is weakly bound to the impurity at low temperatures. This paper is concerned with a donor electron in silicon bound to either an arsenic, a phosphorus, or an antimony impurity. The purpose of this paper is to present the experimental facts obtained from a detailed ENDOR study of these three donors in their ground state. The ENDOR technique developed by Feher[1] can be used to obtain very accurate measurements of the hyperfine interactions between the donor electron and many lattice nuclei. The hyperfine interaction with any one nucleus is expressed in the form of a tensor whose components are the hyperfine constants. In Sec. IV the hyperfine tensors are presented for over 150 lattice sites surrounding *each* of the three donor impurities. These 150 sites per donor are conveniently grouped into about 20 shells per donor.

In a previous investigation,[2] hyperfine tensors for five shells per donor were reported. The present investigation reveals that substantial corrections are necessary for the tensor of shells D and E. In addition, the other three tensors are reported with greater accuracy. The remaining 15 tensors are reported for the first time. We have been able to obtain these new results because different experimental measurement conditions were used which significantly improved the resolution of the ENDOR spectra. In addition, the signal-to-noise ratio was also enhanced.

When the crystal orientation in the magnetic field is varied, the angular dependence of the ENDOR signals permits a unique assignment of an observed shell to the one of three symmetry classes which corresponds to a shell of nuclei at sites on the $\langle 001\rangle$ axes, the $\langle 111\rangle$ axes, and related sites in the $\{110\}$ planes. However, assignments for the majority of the experimental shells to a specific lattice shell within a symmetry class is not possible at this time. For this reason we discuss only the experimental aspects of the problem in this paper. Theoretical considerations concerned with these experimental observations will be discussed in subsequent papers.[3,4]

II. EXPERIMENTAL APPARATUS AND PROCEDURE

A. Samples and Spectrometer Design

The samples were cut from commercially doped single-crystal ingots. Ingots were purchased from Texas Instruments, Inc., and the General Diode Corp. The ingots were specified to be dislocation-free to minimize strain effects which could broaden the ENDOR lines. A typical sample had nominally 8×10^{16} donors per cm^3 and was cylindrical in shape with about a $\frac{1}{4}$-in. diam and a $\frac{1}{2}$-in. length. Cylindrical samples were used to maintain the cylindrical symmetry of the microwave cavity.

The cavity and ENDOR coil arrangement were patterned after that of Seidel.[5] The design is somewhat unusual because the sample, not the magnet, is rotated, and also because the sample is cooled by thermal contact with the inner Dewar rather than immersed in liquid helium. All magnetic resonance signals were detected using a microwave X-band superheterodyne spectrometer with phase-sensitive detection of the audio-modulated signals. The microwave frequency was normally 8770 kMc/sec. The over-all electronic design is described by Gazzinelli and Mieher.[6]

An innovation in the mechanical design for this experiment was the use of a heat shield made of Lucalox.[7]

---

* Work supported in part by the U. S. Army Research Office, Durham, N. C. and the National Science Foundation.

† Present address: Department of Physics and Astronomy, University of Rochester, Rochester, N. Y.

‡ Alfred P. Sloan Foundation Fellow.

[1] G. Feher, Phys. Rev. **103**, 834 (1956).

[2] G. Feher, Phys. Rev. **114**, 1219 (1959).

[3] E. B. Hale and R. L. Mieher, following paper, Phys. Rev. **184**, 751 (1969).

[4] E. B. Hale and R. L. Mieher, Phys. Letters **29A**, 350 (1969) and (to be published).

[5] H. Seidel, Z. Physik **165**, 218 (1961).

[6] R. Gazzinelli and R. L. Mieher, Phys. Rev. **175**, 395 (1968).

[7] Lucalox is a patented name for a polycrystalline alumina material made by the Lamp Glass Division of the General Electric Co.

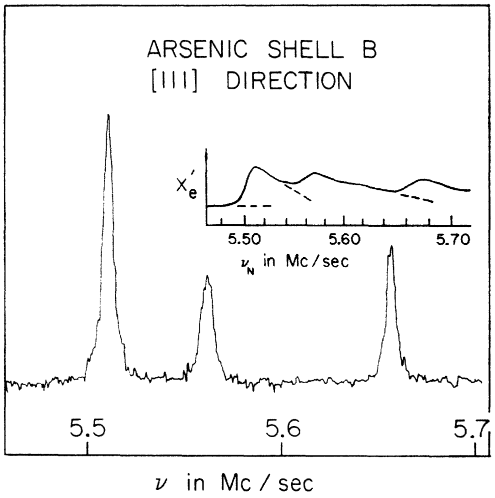

FIG. 1. Recorder traces for shell B in arsenic-doped silicon with $\mathbf{H}_0$ along a [111]-crystal direction. The upper trace is shown by courtesy of Dr. Feher (Ref. 2). The slight difference in the frequency scale between the two traces is not important and occurs because of operation at different microwave frequencies.

The necessity of a heat shield arose since direct exposure of the sample to room-temperature radiation would raise its temperature and would substantially increase the liquid-helium loss rate. The heat shield consisted of a cylindrical tube with a flange on one end and a disk, used as a bottom, on the other. This shield surrounded the sample and was attached to the liquid-nitrogen Dewar via the flange. The shield was constructed of Lucalox since it had the necessary properties of absorption in the infrared range, high thermal conductivity at liquid-nitrogen temperatures, and low dielectric loss.

B. Measurement Procedures

In this experiment a double audio-modulation scheme was found to provide optimum signals. A "high" af (about 400 cps) was used to modulate the large dc magnetic field as in a conventional ESR experiment. A "low" af (about 13 cps) was used to square-wave modulate the ENDOR rf oscillator. The spectrometer was adjusted to observe the dispersion part of the ESR signal. Some ENDOR signals could be observed by sweeping the rf oscillator without the low FM. However, phase-sensitive detection of the low FM eliminated much of the low-frequency noise associated with the large steady-state ESR dispersion signal.

The ENDOR signals differ considerably from those observed by Feher.[2] He observed transient signals which were quite asymmetric due to relaxation effects. We observed symmetrical steady-state signals (i.e., adjusting the oscillator to an ENDOR frequency obtained a constant signal). Figure 1 shows recorder traces from the two experiments. The insert in the upper right corner is taken from Feher's article.[8] Our typical linewidths under high-resolution conditions were 3 kc/sec.

By sweeping the ENDOR oscillator, the spectrum in Fig. 2 was observed. (Assignment of letters to lines is discussed in Sec. IV.) This low-resolution spectrum shows all the high-frequency ENDOR lines and most of the low-frequency lines[9] for an arsenic-doped sample. The smallest number of lines is observed when the magnetic field is along the [001]-crystal direction as shown.

The angular dependence of the spectrum was taken by rotating the sample about the [$\bar{1}$10]-crystal axis. The direction of the dc magnetic field was always perpendicular to this direction; thus the field was always in the crystal-($\bar{1}$10) plane. The direction of the field in this plane will be described by an angle θ rotated from the [001] axis towards the [110] axis. Normally, the high-frequency line spectrum was taken in all three donor-doped samples at every 10° interval in the range $0° \leq \theta \leq 90°$. For regions of the spectrum where severe overlapping of lines occurred, data were taken at 5° intervals or, in some cases, 2° intervals. The frequencies corresponding to over 5000 different line peaks were taken for analysis in this experiment.

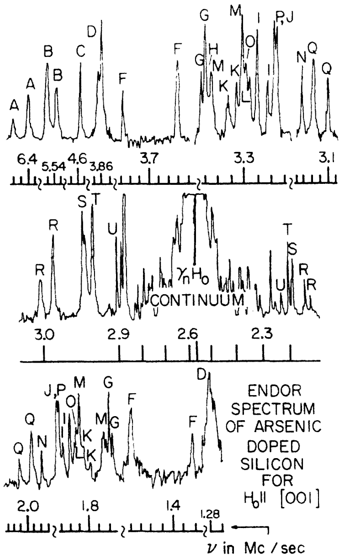

FIG. 2. Recorder traces of ENDOR spectrum in arsenic-doped silicon with $\mathbf{H}_0$ along a [001]-crystal direction. The spectrum was taken on the lowest-field ESR line. The spectrometer gain was occasionally adjusted to better display the data. The frequency interval between the small scale markers is 20 kc/sec. No lines were observed in the omitted frequency intervals.

---

[8] We are indebted to Dr. Feher for permission to use his figure.

[9] The low-frequency lines for shells A, B, and C are not shown because they occur in a frequency region of poor signal-to-noise ratio. There is no doubt, however, that the lines shown for the above shells are the high-frequency lines. This was established definitely by measuring their positive-frequency shift when data were taken on higher-field ESR lines.

III. ANALYSIS OF DATA

A. Hyperfine Interactions

The present experiment is concerned with the ENDOR of silicon nuclei which surround the donor sites. These nuclei are the 4.7%-abundant Si^{29}, which have $I=\frac{1}{2}$ and $\gamma_n=-8.458$ (Mc/sec)/(10 kG). (All other naturally occurring silicon nuclei have $I=0$.)

The data taken in this experiment can be fit to the ENDOR Hamiltonian

$$\mathcal{H}_E=\sum_{\alpha=1}^{N}\mathbf{I}_\alpha\cdot(\mathbf{A}_\alpha\cdot\mathbf{S}-g_n\beta_n\mathbf{H}_0),\tag{1}$$

where α is a parameter which enumerates the lattice sites about the donor, $\mathbf{A}_\alpha$ is the hyperfine-interaction tensor, which relates the nuclear spin $\mathbf{I}_\alpha$ to the electron spin $\mathbf{S}$, and the last term is the nuclear Zeeman interaction.

The tensor $\mathbf{A}_\alpha$ may be separated into the scalar a_α and traceless tensor $\mathbf{B}_\alpha$; thus,

$$\mathbf{A}_\alpha=a_\alpha\mathbf{1}+\mathbf{B}_\alpha,\tag{2}$$

where

$$a_\alpha\equiv\tfrac{1}{3}[(\mathbf{A}_\alpha)_{xx}+(\mathbf{A}_\alpha)_{yy}+(\mathbf{A}_\alpha)_{zz}].\tag{3}$$

In Eq. (2) a_α is the Fermi-contact constant[10] and $\mathbf{B}_\alpha$ is the dipole-dipole tensor. Thus,

$$a_\alpha=(8/3)\pi gg_n\beta\beta_n|\Psi(\mathbf{r}_\alpha)|^2,\tag{4}$$

where $|\Psi(\mathbf{r}_\alpha)|^2$ is the wave-function density at the αth site. At a Si^{29} nucleus, the wave-function density is given by

$$|\Psi(\mathbf{r}_\alpha)|^2=-1.523\times10^{-2}\tfrac{1}{2}a_\alpha\ \text{Å}^{-3},\tag{5}$$

when $\frac{1}{2}a_\alpha$ is expressed in Mc/sec. Also,

$$(\mathbf{B}_\alpha)_{ij}=gg_n\beta\beta_n\langle\Psi|[(3x_ix_j-r^2\delta_{ij})/r^5]|\Psi\rangle,\tag{6}$$

where the expectation value contains the usual dipole-dipole operator.

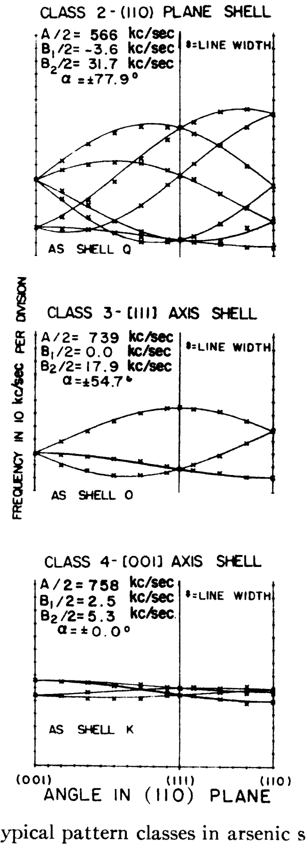

FIG. 3. Typical pattern classes in arsenic spectrum.

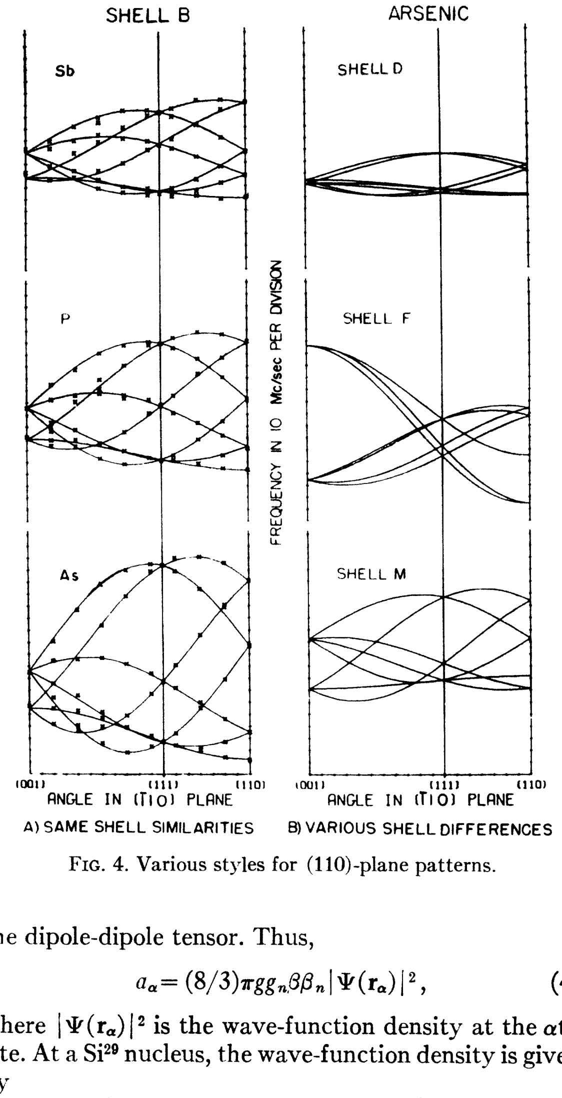

A) SAME SHELL SIMILARITIES B) VARIOUS SHELL DIFFERENCES

FIG. 4. Various styles for (110)-plane patterns.

The ESR data[11] show that $\mathbf{S}$ is essentially parallel to $\mathbf{H}_0$ and, in general, the ENDOR data show that $\mathbf{I}_\alpha$ is also essentially parallel to $\mathbf{H}_0$. Thus, m_s and m_I will be assumed to be good quantum numbers. [Occasionally corrections will have to be made for the above assumptions (see Sec. III E).] By use of the selection rules $\Delta m_s=0$ and $\Delta m_I=\pm1$, the induced ENDOR interaction frequencies can be expressed in the form

$$\nu_\alpha^{\pm}(\theta)=|\gamma_nH_0\pm\tfrac{1}{2}\mathbf{n}\cdot\mathbf{A}_\alpha\cdot\mathbf{n}|,\tag{7}$$

---

[10] E. Fermi, Z. Physik **60**, 320 (1930).

[11] R. C. Fletcher, W. A. Yager, G. L. Pearson, A. W. Holden, W. T. Read, and E. R. Merritt, Phys. Rev. **94**, 1392 (1954); R. C. Fletcher, W. A. Yager, G. L. Pearson, and F. R. Merritt, *ibid.* **95**, 844 (1954).

TABLE I. Properties of the patterns.

	Class 1: unique class	Class 2: {110}-plane class	Class 3: ⟨111⟩-axis class	Class 4: ⟨001⟩-axis class
Site location[a] (n_1,n_2,n_3)	$n_1\neq n_2\neq n_3$	$n_1=n_2\neq n_3$	$n_1=n_2=n_3\neq 0$	$n_1=n_2=0\neq n_3$
Number of sites in the shell	24	12	4	6
Number of lines at general angle in $(\bar{1}10)$ plane	12	7	3	4
Number of S values	3	2	1	2
Number of T values	4	3	2	2
Number of U values	6	4	2	3
Number of independent tensor components	6	4	2	3

[a] *Every* site in the shell must be examined. The shell belongs only to the highest number class possible.

where $\mathbf{n}(\theta)$ is a unit vector along $\mathbf{H}_0$ and the ± arises because of the two possible spin states of the electron. In this experiment the second term on the right side of Eq. (7) seldom exceeds the first term on the right. Figure 2 shows the symmetry of the interaction about $\gamma_n H_0$ which Eq. (7) predicts. Because of the lattice symmetry for a set of α's which form a shell, the frequencies given in Eq. (7) are not independent.

B. Symmetry Considerations

We shall now briefly summarize the results presented in the Appendices. Every nucleus in the crystal can be assigned to a shell. Every shall can be assigned to one of only four possible classes. Every shell class causes a characteristic shell pattern in the angular plot of the ENDOR spectrum (see Fig. 3). The patterns are characterized by the number of S, T, and U values. (These values are the measured frequencies along the [001], [111], and [110] directions, respectively.) The style of a pattern is determined by the magnitudes and signs of the hyperfine interactions. Style is not a unique classification but it is a convenient term for denoting the general appearance of an experimental pattern because the general appearance is similar for the different donors (see Fig. 4).

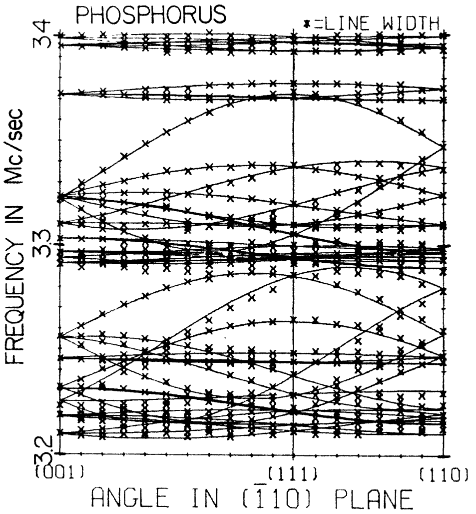

FIG. 5. Angular plot of phosphorus-cluster spectrum.

Figure 3 shows a class-2 pattern, a class-3 pattern, and a class-4 pattern taken from the arsenic spectrum.[12] Figure 4 contrasts the similarities between patterns of the same shell in different donors and the patterns of different shells in the same donor. All six patterns in Fig. 4 belong to {110}-plane shells, i.e., they all have two S, three T, and four U values; the style causes the differences. Figure 4 also illustrates how the same letter assignment can be made in all three donors because of the similarity among the pattern styles. Table I lists the properties of the various patterns.

C. Reduction of Data

After the angular plot of the spectrum is obtained, the various patterns in the data are determined. Sometimes this is a trivial task; sometimes it is not (see Fig. 5). An experienced analyst can usually determine the pattern if *several* lines are well resolved for a range of θ over approximately 40°. The various possible patterns, as well as all the relative line intensities, must be well understood and kept in mind. The analysis is based primarily on the relative line intensities, the possible

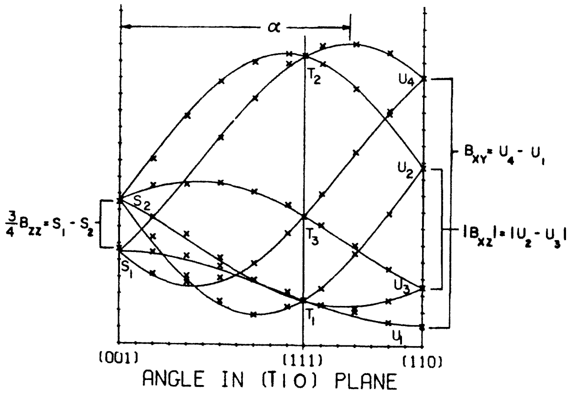

FIG. 6. Some typical relations between the tensor components and the measured S, T, and U values. (These values are defined in Appendix B.)

---

[12] All angular plots shown in this paper—three of which are shown in Fig. 3—were drawn by a Calcomp Plotter with crosses representing a measured line peak and the solid curves, which form the pattern, determined from a four-parameter hyperfine-constant fit for class-2 shells, a two-parameter fit for class-3 shells, and a three-parameter fit for class-4 shells. These plots do not show a very important feature of the lines, namely, the relative intensities.

line combinations, the fact that the lines are $\cos 2\theta$ curves offset from $\theta = 0°$ by a constant angle, and the internal consistency relationships derived by Jung.[13]

Once a pattern has been discovered, the tensor which produced it must be determined. To do this, all the S, T, and U values are used (see Appendix B). Normally there are twice as many of these values as there are independent tensor components (see Table I). To get these components a least-squares fit is made to the S, T, and U values.[14] The fitting procedure, primarily developed by Jung,[13] is exceedingly useful because the S, T, and U values are linearly related to the hyperfine-tensor components expressed in the crystal coordinate system [see Eq. (7) and Fig. 6].

D. Specification of Hyperfine Tensor

At most four independent numbers are needed to express any one hyperfine tensor we have measured. We have found it most convenient to specify a tensor in the crystal coordinate system, where we chose the components for the site at (n_1, n_1, and n_3) as $\frac{1}{2}a$, B_{zz}, B_{xy}, and B_{xz}, where x symbolizes the [100] axis, y symbolizes the [010] axis, and z symbolizes the [001] axis. We also have determined the same tensor in its principal diagonal system by using the parameters $\frac{1}{2}a$, B_{xx}', B_{zz}', and α, where the prime indicates the principal diagonal system.[15] (The directions of the axes and the angle α are defined in the next paragraph.) We also list another set of numbers to describe the tensor, since they were used in the original work by Feher.[2] These numbers are defined as $\frac{1}{2}b_1 \equiv \frac{1}{6}(B_{zz}' - B_{yy}')$ and $\frac{1}{2}b_2 \equiv \frac{1}{6}(B_{xx}' - B_{yy}')$.

For the tensor from every class we have chosen the following: the principal diagonal z' axis to be along the [$\bar{1}$10]-crystal axis; $B_{xx}' \geqslant B_{yy}'$; and α as the angle between the [001]-crystal axis and the principal diagonal x' axis. We can restrict α to the range $|\alpha| \leq 90°$. The above geometry means that

$$B_{xx}' = (B_{xx} + B_{xy}) \sin^2\alpha + B_{zz} \cos^2\alpha + 2\sqrt{2} B_{xz} \sin\alpha \cos\alpha , \quad (8)$$

$$B_{yy}' = (B_{xx} + B_{xy}) \cos^2\alpha + B_{zz} \sin^2\alpha - 2\sqrt{2} B_{xz} \sin\alpha \cos\alpha , \quad (9)$$

$$B_{zz}' = B_{xx} - B_{xy} , \quad (10)$$

and

$$\alpha = \tfrac{1}{2} \tan^{-1}\{-4B_{xz} / [\sqrt{2}(B_{xx} - B_{zz} + B_{xy})]\} . \quad (11)$$

It can be shown[16] that the experiment determines only the absolute values of B_{xz} and α for class-2 tensors and similarly for the B_{xy} component of class-4 tensors. (Whether $\alpha = 0°$ or 90° is related to this B_{xy} ambiguity.)

The tensor components are determined first by the fitting procedure in the crystal system. These components are then used to obtain the components in the other representations. Figure 6 shows a simple way in which the crystal components can be determined by a brief inspection of the pattern.

E. Second-Order Corrections and Error Limits

The $\frac{1}{2}a$ values obtained in the present investigation are as large as several Mc/sec, and the quoted errors are of the order of a few kc/sec. Thus, careful consideration must be given to any effects which can cause the frequencies given in Eq. (7) to depart from the measured frequencies by more than a few parts in 10^{-4}. We have considered corrections which arise from not operating in the ideal high-field limit, where m_s and m_I are precise quantum numbers. One correction arises because of the ENDOR hyperfine interaction itself (the Breit-Rabi correction). A second correction arises because the donor hyperfine interaction mixes in some of the opposite m_s spin state. A third correction arises because of an effective anisotropic internal field which perturbs the spin of the ENDOR nucleus from being along $\mathbf{H}_0$. Except in the case of shell E, these corrections were no greater than the quoted error limits under the conditions of our measurements.[17] The total of all three corrections was applied to a shell if the total correction exceeded 1 kc/sec. For shell E, the third correction is substantial, and can exceed 100 kc/sec in the case of the arsenic donor.

The quoted error limits are based primarily on the reproducibility of the data and the average deviations obtained from the least-squares fitting analysis. The errors in the $\frac{1}{2}a$ values are larger because they are based on an absolute frequency rather than on a frequency difference. Most measurements were taken on two separate occasions often separated by months. At least two samples have been measured for each donor. Measurements have been taken on various ESR lines and on both the high- and low-frequency ENDOR lines. Not all these measurements were of the complete spectrum, nor were they taken with the greatest precision. However, no unexplained effects were found which depended on time, sample, ESR line, or ENDOR line. The precise measurements were analyzed to $\frac{1}{2}$ kc/sec, or better than $\frac{1}{5}$ of a linewidth. The least-squares fit routine typically has an average deviation which is less than $\frac{3}{4}$ kc/sec and never exceeds 2 kc/sec. Errors due to determination of the magnetic field have been considered, but were not important. For shell A, especially in the case of antimony, signal-to-noise problems *primarily* determined the uncertainties in the measurements. For shell E, crystal alignment becomes,

---

[13] W. Jung, Ph.D. thesis, Purdue University, 1963 (unpublished).

[14] The other data points in the angular plots are not normally used to *directly* determine the tensor. They are, of course, used to determine the pattern and the closeness of the final fit.

[15] We have used the short-hand notation that $B_{xx}' \equiv B_{x'x'}$, etc., where the prime axes are in the principal diagonal system.

[16] E. B. Hale, Ph.D. thesis, Purdue University, 1968 (unpublished).

[17] Normally, the precise data were taken on the high-frequency ENDOR line, the low-field ESR line for arsenic and phosphorus, but the high-field ESR line for antimony.

TABLE II. Experimental results for hyperfine tensors in arsenic- , phosphorus- , and antimony-doped silicon. The values are for a positive nuclear g factor. Since Si^{29} has a negative g factor, the values should technically be reversed in sign. All values are in kc/sec except angles, which are in degrees. Absolute value signs occur because signs cannot be determined by ENDOR. Errors in B_{ij} and B_{ij}' are ±10 for shell E and ±2 for the other shells; errors in $\frac{1}{2}a$ are ±10 for shell E and ±3 for the other shells; errors in α are about $\pm1°$ except for shells with small anisotropy, where angle errors are much larger. The continuum cutoff values are 320 kc/sec for As, 300 kc/sec for P, and 305 kc/sec for Sb. The region AAA in the Sb spectrum has $\frac{1}{2}a=415\pm10$ kc/sec and $\lvert\frac{1}{2}b\rvert$ values <10 kc/sec.

Shell class	Donor	$\frac{1}{2}a$	B_{zz}	B_{xy}	$\lvert B_{xz}\rvert$	$\frac{1}{2}b_1$	$\frac{1}{2}b_2$	$\lvert\alpha\rvert$	B_{xx}'	B_{yy}'	B_{zz}'
A ⟨001⟩ axis	As	3860	57.0	$\lvert 55.8\rvert$	0[a]	18.6	23.6	0[a]	57.0	−84.2	27.2
	P	2981	41.4	$\lvert 41.4\rvert$		13.8	17.2		41.4	−62.0	20.6
	Sb	3101	46.0	$\lvert 34.2\rvert$		11.4	17.2		46.0	−57.2	11.2
B {110} plane	As	3000	−41.6	148.2	72.2	−7.4	48.9	67.9	210.4	−83.0	−127.2
	P	2254	−34.0	106.2	39.8	−6.2	32.2	72.2	141.2	−52.0	−89.2
	Sb	1833	−28.6	79.2	20.2	−5.0	22.5	77.5	100.0	−35.0	−65.0
C ⟨111⟩ axis	As	2037	0[a]	5.8	B_{xy}	0[a]	2.9	54¾[a]	11.6	$-\frac{1}{2}B_{xx}'$	B_{yy}'
	P	1649		5.0	B_{xy}		2.5		10.0	$-\frac{1}{2}B_{xx}'$	B_{yy}'
	Sb	1397		6.0	B_{xy}		3.0		11.8	$-\frac{1}{2}B_{xx}'$	B_{yy}'
D {110} plane	As	1292	4.2	20.4	25.4	0.4	12.2	50.6	47.8	−25.2	−22.6
	P	1117	3.6	16.6	22.2	0.7	10.6	50.1	41.0	−22.8	−18.4
	Sb	1003	0.0	17.4	17.4	0.0	8.7	54.6	34.8	−17.4	−17.6
E ⟨111⟩ axis	As	642	0[a]	1258	B_{xy}	0[a]	629	54¾[a]	2516	$-\frac{1}{2}B_{xx}'$	B_{yy}'
	P	270		700	B_{xy}		350		1400	$-\frac{1}{2}B_{xx}'$	B_{yy}'
	Sb	293		522	B_{xy}		261		1044	$-\frac{1}{2}B_{xx}'$	B_{yy}'
F {110} plane	As	1121	151.0	−41.2	4.6	13.8	44.7	1.4	151.2	−116.8	−34.4
	P	840	116.4	−28.2	11.8	9.6	34.2	4.7	117.6	−87.8	−29.8
	Sb	Not present with $\frac{1}{2}a>305$ kc/sec.									
G {110} plane	As	806	7.0	−1.0	5.6	1.0	3.3	27.1	11.2	−8.6	−2.6
	P	764	5.0	−1.2	5.0	1.1	2.8	29.0	9.0	−7.8	−1.2
	Sb	761	4.6	−1.2	5.2	1.1	2.8	30.7	8.8	−7.8	−1.2
H ⟨111⟩ axis	As	801	0[a]	62.4	B_{xy}	0[a]	31.2	54¾[a]	124.8	$-\frac{1}{2}B_{xx}'$	B_{yy}'
	P	689		50.6	B_{xy}		25.3		101.4	$-\frac{1}{2}B_{xx}'$	B_{yy}'
	Sb	703		44.6	B_{xy}		22.3		89.2	$-\frac{1}{2}B_{xx}'$	B_{yy}'
I {110} plane	As	718	−20.4	31.8	12.0	0.5	11.8	75.5	46.2	−24.6	−21.8
	P	685	−17.4	27.8	13.8	0.8	11.1	72.1	42.8	−23.8	−19.2
	Sb	643	−14.0	22.6	14.4	1.1	9.9	68.5	37.6	−22.0	−15.6
J ⟨111⟩ axis	As	694	0[a]	6	B_{xy}	0[a]	3	54¾[a]	12	$-\frac{1}{2}B_{xx}'$	B_{yy}'
	P	739		5.4	B_{xy}		2.7		10.8	$-\frac{1}{2}B_{xx}'$	B_{yy}'
	Sb	Not found									
K ⟨001⟩ axis	As	758	16.0	$\lvert 7.6\rvert$	0[a]	2.5	5.3	0[a]	16.0	−15.6	−0.4
	P	663	14	$<\lvert 12.0\rvert$		...	...		...	...	...
	Sb	Not found									
L {110} plane	As	741	−14.6	9.8	8.2	2.6	6.5	72.0	20.8	−18.2	−2.6
	P	582	−11.2	2.6	7.6	3.2	4.8	66.3	13.0	−16.0	3.0
	Sb	425	−5.8	3.8	4.4	1.3	3.0	67.2	9.6	−8.4	−0.8
M {110} plane	As	777	−60.8	65.2	41.4	7.9	32.8	71.6	115.0	−80.0	−35.0
	P	612	−40.6	49.6	35.6	5.2	25.0	68.8	89.4	−60.2	−29.2
	Sb	559	−37.2	44.0	30.6	4.7	22.0	69.5	78.8	−53.4	−25.4
N ⟨111⟩ axis	As	607	0[a]	4.2	B_{xy}	0[a]	2.1	54¾[a]	8.6	$-\frac{1}{2}B_{xx}'$	B_{yy}'
	P	612		3.4	B_{xy}		1.7		6.6	$-\frac{1}{2}B_{xx}'$	B_{yy}'
	Sb	Not found									
O ⟨111⟩ axis	As	739	0[a]	35.8	B_{xy}	0[a]	17.9	54¾[a]	71.6	$-\frac{1}{2}B_{xx}'$	B_{yy}'
	P	598		32.6	B_{xy}		16.3		65.2	$-\frac{1}{2}B_{xx}'$	B_{yy}'
	Sb	670		31.4	B_{xy}		15.7		62.6	$-\frac{1}{2}B_{xx}'$	B_{yy}'
P {110} plane	As	696	−4.8	4.0	4.2	1.6	2.7	67°	8.8	−7.4	−1.5
	P	662	−6	<6	<6	...	...	...	...	...	...
	Sb	629	...	...	...	<4	<4	...	...	...	...
Q {110} plane	As	566	−48.0	101.6	27.6	−3.6	31.7	77.9	134.0	−56.2	−77.6
	P	524	−40.2	84.0	22.8	−2.8	26.4	77.9	111.0	−47.2	−64.0
	Sb	387	−36.0	78.6	31.6	−1.9	26.7	73.0	110.4	−49.6	−60.8
R {110} plane	As	428	24.8	0.0	25.0	3.6	13.4	31.2	46.2	−33.8	−12.4
	P	379	21.0	0.2	19.4	2.6	10.5	30.1	36.8	−26.0	−10.8
	Sb	332	15.0	−2.8	12.0	2.4	7.1	26.5	23.6	−18.8	−4.8

TABLE II (*continued*)

Shell class	Donor	$\frac{1}{2}a$	B_{zz}	B_{xy}	$\lvert B_{xz}\rvert$	$\frac{1}{2}b_1$	$\frac{1}{2}b_2$	$\lvert\alpha\rvert$	B_{xx}'	B_{yy}'	B_{zz}'
S {110} plane	As	377	−5.4	9.2	0.0	−0.2	2.9	90	12.0	−5.4	−6.4
	P	410	−5.4	7.4	0.0	0.1	2.6	90	10.0	−5.4	−4.8
	Sb	525	−5	<4	<4	...	...	...	...	...	...
T {110} plane	As	364	0.0	4.4	4.4	0.0	2.2	55	8.6	−4.4	−4.4
	P	398	0.0	3.8	4.2	0.1	2.1	54	8.2	−4.4	−3.8
	Sb	Not found									
U {110} plane	As	338	...	...	...	<2	<2	...	...	...	...
	P	383	...	...	...	<2	<2	...	...	...	...
	Sb	Not found									
V {110} plane	As	Not present with $\frac{1}{2}a>320$ kc/sec.									
	P	Not present with $\frac{1}{2}a>300$ kc/sec.									
	Sb	504	37.0	0.2	30.2	3.8	17.0	28.5	60.2	−41.6	−18.6
W {110} plane	As	Not found									
	P	328	...	...	...	<2	<2	...	...	...	...
	Sb	Not found									
X {110} plane	As	242	40	30	...	...	...	...	...	...	...
	P	317	29.4	23.6	32.2	−1.8	15.6	38.7	65.8	−27.6	−38.4
	Sb	437	20.4	19.0	20.8	−2.3	10.0	39.5	44.6	−15.4	−29.2

[a] Determined by symmetry.

quite important and increases the error limits. For shells of small anisotropy, uncertainties due to overlapping of lines become very important.

IV. RESULTS

The experimental results for all three donors are tabulated in Table II.[18] Table III compares the previous results[2] and the present results. Significant differences exist for shells D and E and will be discussed below. The previous work[2] also assigned the shells to the lattice shells from which they apparently arose. This *theoretical* aspect of the problem is considered in subsequent papers.[3,4]

A. General Remarks

The most detailed study of the spectrum was in the arsenic samples, since they yielded the largest signal to-noise ratios and since the arsenic shells have the

TABLE III. Comparison of previous results[a] and present results.

Shell	Class[a]	Site assignment[a]	Donor	$\frac{1}{2}a$ Mc/sec		$\frac{1}{2}b_1$ kc/sec		$\frac{1}{2}b_2$ kc/sec		α Deg	
				Previous	Present	Previous	Present	Previous	Present	Previous	Present
A	⟨001⟩ axis	(0,0,4)	As	3.86	3.860	20	18.6	23	23.6	0.0^b	0.0^b
			P	2.98	2.981	14	13.8	17	17.2		
			Sb	3.10	3.101	8	11.4	15	17.2		
B	{110} plane	(4,4,0)	As	3.00	3.000	−6	−7.4	52	48.9	67	67.9
			P	2.26	2.254	...	−6.2	28	32.2	71	72.2
			Sb	1.83	1.833	...	−5.0	24	22.5	75	77.5
C	⟨111⟩ axis	(3,3,3)	As	2.04	2.037	0.0^b	0.0^b	4	2.9	54.75^b	54.75^b
			P	1.64	1.649			<4	2.5		
			Sb	1.39	1.397			<4	3.0		
D	⟨111⟩ axis[c]	(5,5,5)[d]	As	1.29	1.292	$0.0^{b,d}$	0.4	12	12.2	$54.75^{b,d}$	50.6
			P	1.13	1.117		0.7	10	10.6		50.1
			Sb	1.01	1.003		0.0	8	8.7		54.6
E	⟨111⟩ axis	(1,1,1)	As	0.80	0.642	0.0^b	0.0^b	550	629	54.75^b	54.75^b
			P	...	0.270			...	350		
			Sb	0.60	0.293			120	261		

[a] G. Feher (Ref. 2.).
[b] Required by symmetry.
[c] Present experiment shows this to be (110)-plane-class shell.
[d] Present experiment shows this to be impossible.

---

[18] A limited number of booklets have been prepared which show the measured-shell patterns for about 50 shells. These booklets are available upon special request to either of the authors.

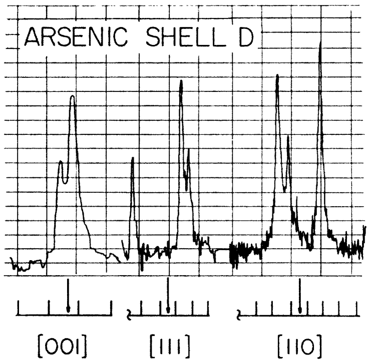

FIG. 7. Simple crystal-axes spectra for shell D in arsenic-doped silicon. The present experiment revealed the splitting of the overlapping lines. Arrows on frequency scale indicate $\gamma_n H_0 + \frac{1}{2}a$.

largest anisotropy. The lettering of the shells was essentially done in descending order with $\frac{1}{2}a$ values in the arsenic spectrum. The lettering in the case of the other two donors was done following the similarity of the pattern style to a style in arsenic. If no similar style was found, the next available letter was used.

The regions where $\frac{1}{2}a < 320$ kc/sec in arsenic, $\frac{1}{2}a < 300$ kc/sec in phosphorus, and $\frac{1}{2}a < 305$ kc/sec in antimony have been somewhat artificially named the "continuum," since the lines form essentially a continuous spectrum, being severely overlapped and entangled from these $\frac{1}{2}a$ cutoff values to zero. We believe that the existence of any shell whose $\frac{1}{2}a$ value is above the appropriate continuum cutoff value and which is not discussed in Sec. IV B is very unlikely.

The lettering of the shells between donors done following the similarity of the style is considerably more reliable for some shells than for others, depending primarily on the strength of the anisotropy. For shells of large or intermediate-size anisotropy there seems little doubt about the letter matching. (These shells are A–F, I, K, M, Q, R, V, and X.) For shells of small anisotropy the style is very poorly defined, and a letter simply designates the existence of a shell. (These shells are G, L, P, S, T, U, and W.) Primarily from intensity considerations, we believe that all of the above shells of small anisotropy belong to the {110}-plane class of shells. We can not, however, completely rule out that they do not obscure another shell of small anisotropy from the ⟨001⟩-axis class or the ⟨111⟩-axis class, since the total intensity for either of these classes is significantly smaller than for the {110}-plane class. In particular, the "absence" of shells K, J, and N from the antimony spectrum could possibly be caused by any one of them being obscured by shells G or P. In the discussion of the individual shells, other possible interpretations of the data are discussed.

The most distinctive or unusual characteristic feature or features of the shells are also mentioned in these discussions. Normally for the same lettered shells, the $\frac{1}{2}a$ values and the pattern styles approximately "scale-down" in the order, arsenic, phosphorus, antimony (see Fig. 4a). Exceptions to this general rule are noted.

B. Discussion of Individual Shells

Shell A. This shell[19] is one of only two ⟨001⟩-axis shells resolved. The large nonaxial dipole-tensor characteristics are noteworthy.[20] Also, an anomaly occurs in that $\frac{1}{2}a_{\text{Sb}} > \frac{1}{2}a_{\text{P}}$.

Shell B. (See Fig. 4.) This shell[19] and shell F have the largest dipole-tensor components in the {110}-plane class of shells.

Shell C. This[19] is the first of the six ⟨111⟩-axis class of shells, yet it has a rather small anisotropy.

Shell D. (See Fig. 4.) This[19] is a {110}-plane shell which has a style quite similar to the ⟨111⟩-axis-class pattern. The original error in identification of this pattern arose because of this feature. If intensities are not considered, a ⟨111⟩-axis pattern is a special case of a {110}-plane pattern. Contrast shell D in the upper right angular plot in Fig. 4 with the center plot of Fig. 3. Our improved resolution has definitely shown that this shell cannot be a ⟨111⟩-axis pattern. Figure 7 shows an actual recorder trace of the shell-D spectrum in arsenic along the three simple directions. The newly observed structure is the splitting between the overlapping lines. It is impossible that the "new" splittings are due to crystal misalignment since a proper alignment of better than $\frac{1}{2}°$ is known to exist from measurements on the other shells. Furthermore, the intensity of the signals agrees well with a shell having a total of 12 nuclei (class 2) rather than four nuclei (class 3). In phosphorus the splitting is smaller, as expected, but can still be detected. For antimony, where the signal-to-noise ratio is worse and the anisotropy smaller, only line broadenings for the new splittings were observed. From intensity considerations, as well as from relative

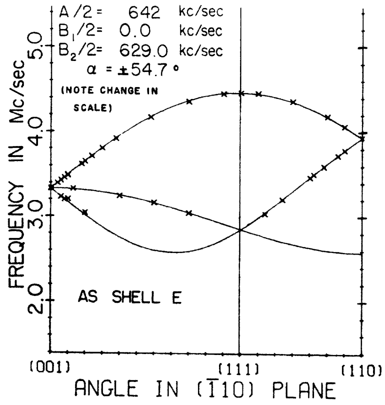

FIG. 8. Angular plot for shell E in arsenic-doped silicon. The frequency scale is 200 kc/sec per division.

---

[19] This shell was previously reported in Ref. 2.

[20] In the principal coordinate system, axial-tensor characteristics occur when $B_{yy}' = B_{zz}'$ or, equivalently, if $\frac{1}{2}b_1 = 0$; large nonaxial characteristics occur when $|\frac{1}{2}b_1| \gtrsim \frac{1}{2}b_2$.

locations in the spectrum, it seems most likely that the observed pattern in antimony is from shell D.

Shell E. (See Fig. 8). This[19] is a shell with dipole-tensor components an order-of-magnitude larger than those of any other shell. This shell exhibits the donor anomaly in that $\frac{1}{2}a_{\mathrm{Sb}} > \frac{1}{2}a_{\mathrm{P}}$. Feher apparently only resolved a 40° interval for the upper line of this shell in arsenic and presumably a smaller interval in antimony.[2] His results for the tensor components are in rather marked disagreement with those of the present investigation. The crosses in Fig. 8 show the lines we were able to measure above the continuum. (The frequency scale of Fig. 8 is 200 kc/sec per division, 20 times larger than the frequency scale used in all our other angular plots.) The pattern lines represent the fit obtainable with our hyperfine constants, where anisotropic corrections have been applied. [These corrections were of the same form as given in Ref. 2, Eq. (13)]. Inspection of the data presented in Ref. 2 shows that the few points measured are *not* in disagreement with the present measurements. It thus appears that our numbers are within the original unstated error limits. It is not understood why this shell was not previously observed in the phosphorus spectrum.

Shell F. (See Fig. 4). This shell has two distinctive features. One is that it is missing in antimony. (Perhaps it should be mentioned that shell V is a shell with rather large dipole constants which are found only in antimony; the style of shell V is quite distinct from that of shell F, however.) The second feature is that it is the only shell with a large ***negative*** B_{xy}.

Shell G. This is a shell with a small anisotropy. Although all the lines overlap, all S and T values are resolved. The line intensities are in good agreement with a 12-nuclei (class-2) shell; the S, T, and U values are also consistent with this class of shell pattern. It seems rather unlikely that this shell is not a single shell with a {110}-plane symmetry. What little style there is seems consistent in all three donors, i.e., $T_2 > T_1 > T_3$ and $S_1 > S_2$.[21]

Shell H. Shells H and O are both ⟨111⟩-axis-class shells with an intermediate size anisotropy (see Fig. 3). In all three donors shell H has the largest $\frac{1}{2}a$ and B_{xy} values when compared with shell O. This is a pleasant consistency but it does not guarantee that the shell matching is unique in the different donors. Note again that $\frac{1}{2}a_{\mathrm{Sb}} > \frac{1}{2}a_{\mathrm{P}}$ for both shells.

Shell I. Shell I has its S, T, and U values rather uniformly distributed and a small nonaxial character.

Shell J. Both shells J and N have small anisotropy and are ⟨111⟩-axis patterns. The fact that they are class-3 rather than class-2 shells is principally determined by their line intensities, which are consistent with a shell having four rather than 12 nuclei. They are almost identical to shell C, which is only distinguished from them by its large $\frac{1}{2}a$ value. Both shells are easily seen in the phosphorus spectrum. In the arsenic spectrum shell N is easily seen, but shell J is essentially obscured by shell P, which has a much stronger over-all intensity and occurs at almost the identical frequency. Because of this fact, shell J is a marginal identification in arsenic. (See shell P for further discussion of this point.) Neither of these shells was observed in antimony. It is possible that one or both shells occurs in the AAA region; or even that shell G or P could obscure one of them.

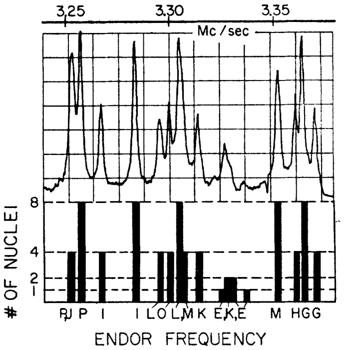

Fig. 9. High-resolution arsenic-cluster spectrum along the [001]-crystal axis. The lower portion of the figure shows the analysis based on the additional data contained in the complete angular plot. The sum of the total number of nuclei should be proportional to the observed line intensity.

Shell K. (See Fig. 3.) This shell is the second of two observed shells in the ⟨001⟩-axis class. Unfortunately, the shell exists in a region of strong line overlapping in both arsenic and phosphorus and was not found in antimony. (It is possible that it is obscured by shell P or region AAA.) The class-4 shell pattern is the only case where an S value can exist with an absolute intensity of 2, and it is primarily on this basis that the shell is best identified. In arsenic the spectrum near shell K has been studied in great detail. (See discussion of cluster in arsenic spectrum.) Shell K definitely exists in this region, but it is necessary to assign somewhat greater uncertainty to the dipole constants. In phosphorus, because of the overlap with shell P, only S_1 and T_1 could be uniquely determined, and thus no dipole constants could be assigned. The style of the pattern does seem consistent with the style in arsenic, however.

Shell L. This shell[22] is consistent with a class-2 pattern having a rather small anisotropy, with $S_2 - S_1 \sim 5$ to 10 kc/sec and $T_1 \sim T_3$. In all donors this shell overlaps with other shells. It is in the middle of the cluster regions in both arsenic and phosphorus and defines the upper AAA region in antimony. The dipole constants are thus considerably more uncertain than in most other shells. The matching of the shell between the various donors is rather speculative, and should not be considered certain.

---

[21] These symbols are defined in Appendix B.

[22] The style and anisotropy of shells L, P, S–U, and W are poorly defined; thus, in these cases, the lettering of a shell designates that a shell exists at such a frequency, but we do not guarantee that the same lettered shell in different donors is properly mated. (See. IV B.)

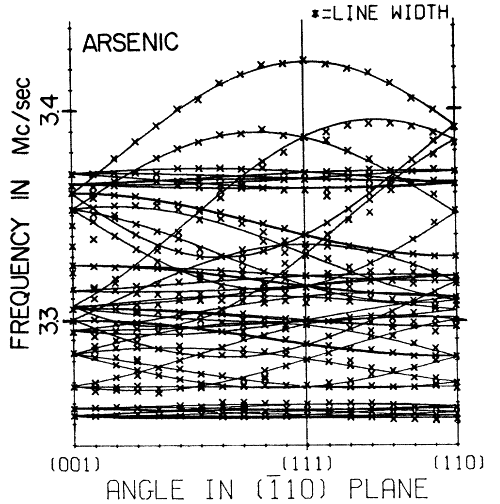

FIG. 10. Angular plot of arsenic-cluster spectrum.

Shell M. (See Fig. 4.) This class-2 shell has a well-defined style which is quite similar to the style of shell B.

Shell N. See shell J.

Shell O. See shell H.

Shell P. This shell[22] has a small anisotropy with $S_2 > S_1$. The intensities and pattern are not inconsistent with a class-2 shell. This shell really designates the existence of a pattern in a given donor at the stated $\frac{1}{2}a$ value rather than a matching of shells between donors. In arsenic the two S-value lines have the relative number of nuclei intensities of 8±2 and 7±2 and are somewhat overlapping (see Fig. 9); the three T values have apparent intensities of 5±2, 8±2, and 8±2 and are well overlapped. Because of the almost equal S values, it seems possible that a ⟨111⟩-axis shell overlaps the weakest S value and gives it almost an intensity of 8 rather than the normal value of 4. The T and U values are consistent with this interpretation. Shell-P and shell-J assignments are based on the above considerations and should be considered somewhat marginal. In phosphorus the shell-P anisotropy is so small that all the T values appear as one more or less symmetric broad line. No dipole constants have been assigned; it is definite, however, that $S_2 > S_1$, and it appears[23] likely that $T_2 > T_1 > T_3$. In antimony shell P is rather poorly resolved and, in addition, it is somewhat entangled with shell I. The intensities of the lines are slightly greater than those expected from a {110}-plane-class shell. We guess that this shell is a {110}-plane-class shell and is quite possibly entangled with a ⟨001⟩-axis-class shell or a ⟨111⟩-axis-class shell of small anisotropy.

Shell Q. (See Fig. 3.) This shell has an intermediate-size anisotropy and is somewhat similar in style to shell M.

Shell R. This shell is most easily distinguished by the accidental degeneracy of the U_1, U_3, and U_4 values.

Shell S. Shell S is[22] of rather small anisotropy with $S_2 > S_1$ and $T_2 \sim T_3$. Due to the overlap of T_2 and T_3, there are only two observed T values. Thus, there is some uncertainty as to which of the two nearly equal T values is T_1. In both arsenic and phosphorus the lowest T value has about a one-part-in-six greater intensity, and the analysis assumes that this was the T_1 value. In antimony, none of the T values are distinct. This condition is similar to that found for shell P in phosphorus.

Shell T. This shell[22] has a pattern similar to a ⟨111⟩-axis shell, but the intensity is that of a {110}-plane shell. In this respect its pattern is similar to the shell-D pattern as seen by Feher (see discussion of shell D). It was not found in antimony, but could exist in the AAA region.

Shell U. Shells U and W are[22] completely unresolved isotropic lines of apparent intensity 12±4 and are thus most likely of the {110}-plane class.

Shell V. This shell was found only in antimony, and its style is quite similar to shell R except that its dipole constants are larger. The fact that such a large anisotropic shell could not be found in the other two donors may indicate that it is the missing shell F in antimony with a considerable change in style.

Shell W. See shell U.

Shell X. Shell X has rather well-distributed set of S, T, and U values and is readily found in phosphorus and antomony. A search of the upper continuum in arsenic indicates that a tentative value for $\frac{1}{2}a$ can also be assigned in this donor. Certain features of the pattern style can be observed, but overlap with several other shells makes dipole-constant assignments difficult. This shell is very unusual in that the $\frac{1}{2}a$ values scale up from arsenic to phosphorus to antimony.

Region AAA. There[24] exists in antimony a region (approximately 20 kc/sec wide) of several very intense lines. Shell L was resolved from the upper half of the region. The lower half of this region could not be definitely resolved. Perhaps this lower region is just one shell of class 1. Perhaps, also, it is two or more shells of class 2 or lower symmetry which badly overlap and, in addition, have a small anisotropy. It is possible that a few weak lines could be entangled with shell L.

C. Discussion of Clusters

Some of the observed patterns overlap. Regions of strong overlap have been named clusters and are discussed below.

Arsenic cluster. For $\mathbf{H}_0$ along [001] or $\theta = 0°$ the high-resolution arsenic-cluster spectrum is shown in Fig. 9.[25]

---

[23] Shell S in antimony also has $S_2 > S_1$ and the same T characteristics.

[24] We decided to designate regions where lines badly overlapped and could not be resolved with three letters which descend from AAA; a considerable number of these regions are likely to be found when a detailed study of the continuum is carried out.

[25] For contrast consider the low-resolution conditions of Fig. 2, which contains the same spectrum.

The angular plot for the arsenic cluster is shown in Fig. 10. The cluster spectrum consists of the shells G–P, and for θ near 0°, shell E.[26] (None of the other resolved shells in the arsenic spectrum are badly overlapped.) How these shells were untangled will now be discussed using Figs. 9 and 10. The highest shell of small anisotropy is shell G; it is not badly overlapped and is readily determined. Shell H is the "fat" shell having the highest T value in the cluster. (This one-line T value readily identifies a $\langle 111 \rangle$-axis pattern since this is the only T value formed by one line in any of the classes.) The next-lowest T value belongs to shell M; its large anisotropy makes it easy to resolve, although it overlaps with several other shells. Shell K (consider Fig. 10 in conjunction with Fig. 9) was determined by taking data every 2° for the interval $0° < \theta < 40°$. The lines leaving the unusually weak S_1 value of this $\langle 001 \rangle$-axis shell can be clearly followed over this angular region. In addition, one of the lines leaving the S_2 value can also be followed. The lines for shell E are not drawn on the plot. The unconnected crosses near shell K at 0° are the only resolved shell-E lines in the cluster. As the angle is changed, the shell-E lines rapidly diverge from their 0° value and leave the cluster region. Shell L was determined by intensity considerations and by processes of elimination. Shell I consists of the lowest two S values above shell P and is rather easily resolved. Shell O was originally determined by the line segments which go through the shell-I spectrum. The lowest series of lines with small anisotropy are shells J and P, and their entanglement has previously been considered (see Sec. IV B, shell P).

The lower portion of Fig. 9 shows a bar graph of the final, analyzed, *expected* relative intensities. Note how reliable the intensities are. Computer programs have been written which for every 10° interval plot the spectrum based on the hyperfine constants assigned to the shells and the expected relative intensities of the many lines. A detailed analysis for $0° < \theta < 90°$ shows that no predicted or observed lines are unaccounted for—a strong indication of a correct analysis—and, furthermore, the line intensities are all in reasonable agreement with the observed values. The data have been carefully analyzed at every 5° interval, and any substantial error in analysis seems very unlikely except for those possibilities mentioned in Sec. IV B.

Phosphorus cluster. Figure 5 shows the phosphorus cluster which contains shells G–P, and over small-angle intervals near 20° and also near 85°, one line from shell E (which is not drawn in the figure). The spectrum is considerably less complex than in arsenic. The top series of crosses is the isolated shell G. Below it, shell J is also well isolated. Shell H is readily apparent as the single-line T value near shell J. Shell I is the clearly resolved shell with one S value near that of shell H. Shells K and P strongly overlap in about the center of the spectrum. Shell K is distinguished by its unusually weak S_1 value. Shell M is the next lower shell determined by its large and clear style. Shell O is readily distinguished by its single-line T value. Shell N is the shell of small anisotropy through the middle of shell M. Shell L is the lower series of crosses. Data analysis has been carried out for every 5° interval, and there appears little chance of error except as previously discussed for the shells with small anisotropy.

(It should be mentioned that the phosphorus shells R–U, W, and X are not completely isolated, but form a spectrum of even less complexity than the cluster spectrum.)

Antimony cluster. The spacing of the shells is more uniform in the case of antimony except in the AAA region. There exists overlapping, but it introduces few problems in resolving the spectrum.

V. SUMMARY

The hyperfine interactions of about 20 shells for each of three donors in silicon have been measured by ENDOR. Over 175 *independent* hyperfine constants were reported in this paper. We have determined the donor-electron hyperfine interaction for two shells along the $\langle 001 \rangle$ axes (shells A and K); for six shells along the $\langle 111 \rangle$ axes (Shells C, E, H, J, O, and N); and for about 10 shells at other locations in the $\{110\}$ planes. These data will provide a great deal of information on the donor wave function when the shells can be uniquely correlated with the actual lattice shells. Unfortunately, at this time very few unique shell assignments can be made even with the division of the shells into three symmetry classes. For this reason, this paper presents just the experimental facts. Subsequent papers[3,4] will contain our interpretation of the data and some theoretical considerations regarding these hyperfine interactions.

APPENDIX A: SHELLS, CLASSES, AND HYPERFINE TENSORS OF LATTICE NUCLEI

Any lattice site about the donor can be specified by a set of coordinate integers (n_1,n_2,n_3), if the units of length for the coordinate system is a lattice constant a_0 divided by 4 (see Fig. 11). It is often convenient to specify the lattice nuclei by grouping them into a series of shells which surround the donor.[27] (A shell is formally defined in Appendix B). The shell radius is given by[28]

$$R \equiv (n_1{}^2 + n_2{}^2 + n_3{}^3)^{1/2} \tfrac{1}{4} a_0 . \qquad (12)$$

---

[26] In this figure, the shell-E lines appear as three unconnected crosses which are split because of a slight ($<\frac{1}{2}°$) crystal misalignment.

[27] A more detailed treatment of the subjects discussed in the Appendices is contained in Ref. 16.

[28] Sometimes there is more than one shell at the same radius. This can happen in two distinct ways. One is caused by a numerical "accident" such as for the (333) and (115) shells. The second occurs because every even-integer site has its inversion-related site occupied. Since inversion is not an operator of the crystal point group about the impurity site, two distinct shells should be considered. (An exception to this occurs if any site coordinate is zero; then, only one shell need be considered.)

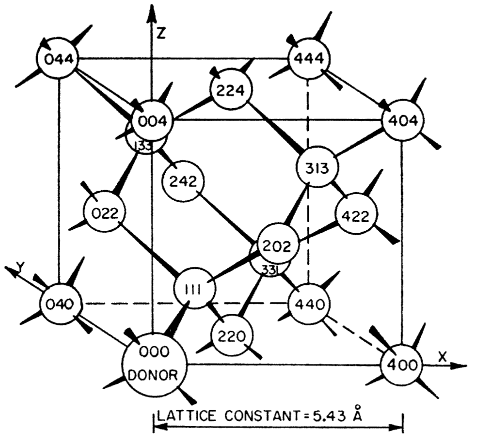

SITE COORDINATES ARE IN SILICON UNITS.

FIG. 11. Crystal coordinate system and lattice sites about a donor impurity.

In each shell there are several nuclei which are located at the *occupied* positions corresponding to the permutations of the integers $\pm n_1$, $\pm n_2$, and $\pm n_3$. Consideration of the lattice shows that (1) if all the coordinate integers are distinct, i.e., $n_1 \neq n_2 \neq n_3$, then there are 24 nuclei per shell; (2) if only two of the integers are equal, then there are 12 nuclei per shell; (3) if all the integers are equal, then there are four nuclei per shell; and (4) if two integers are equal to zero, then there are six nuclei per shell. Consideration of the above four classes shows that every shell in the lattice must be a member of one of the classes. We will refer to the above shell classes as follows: class 1—unique class, class 2—{110}-plane class, class 3—⟨111⟩-axes class, and class 4–⟨001⟩-axes class. Let a tensor **A** be associated with a lattice nucleus and be expressed in the crystal-axis coordinate system (see Fig. 11). There are only six independent components of **A** because of the physical requirement that $A_{ij}=A_{ji}$ for i or $j=x$, y, or z. If the nucleus with tensor **A** is a member of a shell belonging to a class other than the unique class, the symmetry of the lattice requires that the above six components of **A** no longer be independent. It can be shown that for a site in the $(\bar{1}10)$ plane (class 2) $A_{xx}=A_{yy}$ and $A_{xz}=A_{yz}$. Thus, there are only four independent components, which we take to be A_{xx}, A_{zz}, A_{xy}, and A_{xz}. For a site along the [111] axis (class 3), there are two independent components A_{xx} and A_{xz}, since, in addition to the class-2 restrictions, $A_{xx}=A_{zz}$ and $A_{xy}=A_{xz}$. For a site along the [001] axis (class 4), there are three independent components A_{xx}, A_{zz}, and $A_{xy}=A_{xz}$.

APPENDIX B: ENDOR PATTERNS AND STYLES OF SHELLS

We define a shell as a collection of lattice nuclei whose hyperfine tensors are *not* independent. Namely, given the tensor for one nucleus, the tensors for every other nucleus in the same shell are uniquely determined.[29] The tensors are related, of course, because of the symmetry between the lattice and the defect. Because the tensors from nuclei in a given shell are not independent, the ENDOR lines from these nuclei form a characteristic pattern as the magnetic field is rotated. Each of the four shell classes has a distinct pattern. *Thus, an ENDOR pattern determines to which of the four classes the observed shell belongs.*

TABLE IV. Pattern degeneracies at various S, T, and U values.

	S_1	S_2	T_1	T_2	T_3	U_1	U_2	U_3	U_4
{110}-plane class	4	8	6	3	3	2	4	4	2
⟨111⟩-axis class	4	···	3	1	···	···	2	2	···
⟨001⟩-axis class	2	4	3	3	···	1	3	···	1

The patterns are characterized by the symmetry-required degeneracy of at least two ENDOR lines when the magnetic field is aligned along a direction of high crystal symmetry. These directions are [001], [111], and [110]. We designate the frequencies for one pattern along these three directions by S_i, T_j, and U_k, respectively.[30] For class 1, there are three S values, four T values, and six U values; for class 2, there are two S values, three T values, and four U values; for class 3, there are one S value, two T values, and two U values; and for class 4, there are two S values, two T values, and three U values. For other than Class 1, we define the following: $S_1 \equiv S$ value of least degeneracy,[31] $S_2 \equiv S$ value of greatest degeneracy, $T_1 \equiv T$ value of greatest degeneracy, $T_2 \equiv T$ value of highest frequency excluding T_1, $T_3 \equiv T$ value of lowest frequency excluding T_1, $U_1 \equiv U$ value of line through S_1 and T_1, $U_2 \equiv U$ value of line through S_2 and T_2, $U_3 \equiv U$ value of line through S_2 and T_3, and $U_4 \equiv U$ value of the loop leaving S_1. Figure 6 shows a class-2 pattern and the above-defined S, T, and U values. Table IV lists the pattern degeneracies at the various S, T, and U values. The properties of the pattern classes are summarized in Table I.

We refer to characteristic features of a pattern as the pattern style. This is not a rigorous concept, but it is useful, especially to distinguish between patterns belonging to the same class. The pattern arises because of the lattice and defect symmetries; the style is due to details of the electron wave function which are not required by symmetry.

---

[29] One tensor is obtained from any other by performing a similarity transformation using the rotation operator, which transforms the two nuclei into each other but does not alter the lattice and defect structure.

[30] These definitions and many of the results which follow from them were originally used by Jung (Ref. 13) to analyze ESR patterns. We have made minor modifications and have applied them to our ENDOR patterns.

[31] Under ideal measurement conditions, degeneracy and line intensity are proportional.